Formation of the *MAX*-phase oxycarbide $Ti_2AlC_{1-x}O_x$ studied via electron energy-loss spectroscopy and first-principles calculations

P. O. Å. Persson,[1] J. Rosén,[1] D. R. McKenzie,[2] and M. M. M. Bilek[2]
[1]*Thin Film Physics, Linköpings Universitet, 58183 Linköping, Sweden*
[2]*School of Physics, University of Sydney, New South Wales 2006, Australia*
(Received 17 February 2009; published 15 September 2009)

Oxygen incorporation in the Ti_2AlC *MAX* phase and TiC was investigated in the electron microscope using spatially resolved fine-structure electron energy-loss spectroscopy analysis. Corresponding fine structures were calculated within the full-potential-linearized augmented plane-wave framework. In the calculations, oxygen was substituted for aluminum and carbon in Ti_2AlC as well as for carbon in TiC, in concentrations of 3.1, 6.2, and 12.5 at %. Comparison of calculated and measured spectra shows that oxygen is incorporated on the carbon site in both TiC and Ti_2AlC. These findings reveal the existence of *MAX* phase oxycarbide $MA(O,C)$ alloys and O as a third *X* element in addition to C and N.

DOI: 10.1103/PhysRevB.80.092102 PACS number(s): 79.20.Uv

$M_{n+1}AX_n$ phases are a family of nanolaminated ternary materials,[1] where *M* is an early transition metal, *A* is a group IIIA or IVA element, and *X* was until recently believed to be carbon and/or nitrogen only.[2,3] These materials have recently attracted increased attention due to their unique combination of metallic and ceramic properties. Although synthesized primarily as bulk materials,[4] they have also been prepared by thin-film growth, using magnetron sputtering as well as cathodic arc deposition.[5,6]

Presently, around 60 "pure" *MAX* phases, of which about ten are nitrides, have been synthesized. A large number of MAX phases have also been synthesized by *M* and/or *A*-site alloying, e.g., $(Ti,V)_2AlC$ or $Ti_3(Al,Sn_{0.2})C_2$.[2,7,8] Here, the incentive is to reach alloy properties which deviate from a mixture of the corresponding two phases. This hypothesis has been confirmed by both theoretical and experimental, results with, e.g., an increased hardness of the alloy.[9,10] *X*-site alloys are less common but $Ti_2Al(C,N)$ and $Ti_3Al(C,N)_2$ have, for example, been investigated.[8,11] Naturally, the permutation space is limited if *X* is restricted to two elements only.

Recent investigations have shown that *MAX*-phase thin films can incorporate significant levels of oxygen (>15 at %) while apparently retaining the *MAX* crystal structure.[12,13] Residual gas impurities which are present during physical vapor deposition have been suggested as a possible source for the incorporated oxygen.[13] A second source recently suggested is the decomposition of an Al_2O_3 substrate.[12] However, *MAX* phases such as Ti_2AlC, typically contain a small amount of cubic TiC, which is known to readily incorporate oxygen by the formation of an oxycarbide.[14] Grain boundaries and structural imperfections are also known to getter oxygen,[15] hence it is not yet clear whether the oxygen is actually incorporated in the *MAX* structure, in the TiC residual or both. A previous investigation demonstrated an anticorrelation between carbon and oxygen along a concentration depth profile, which suggests oxygen substitution on carbon sites.[13] However, this is in contradiction with a theoretical investigation suggesting that corresponding substitution in Ti_3SiC_2 results in structural instability.[16] Also, in a recent study, oxygen was suggested to be incorporated as an interstitial, causing Al vacancy formation.[17]

If the oxygen is in fact incorporated in the *MAX* crystal structure, adjusting its concentration presents a new alloying opportunity to tailor the material's properties. However, in order to predict and tailor new properties, through theoretical approaches, an understanding of the oxygen incorporation in the structure is required.

In this Brief Report, the incorporation of oxygen in Ti_2AlC and TiC is investigated experimentally and theoretically using spatially resolved electron energy-loss spectroscopy (EELS) spectrum imaging and first-principles computational methods. Specific attention is given to the fine structure of the oxygen *K* edge. It is shown, by comparing experimental and theoretical data, that oxygen is incorporated on the carbon site in both Ti_2AlC and TiC. This finding reveals O as a third *X* element, indicates the existence of *MAX*-phase oxycarbides, and proposes, in analogy to pure $MA(C)$ and $MA(N)$ phases, the existence of a $MA(O)$ phase.

A single epitaxial thin film containing Ti_2AlC and TiC phases was deposited on an Al_2O_3 substrate using a filtered cathodic arc source, described elsewhere.[18] By x-ray diffraction methods, the deposited phases were found to assume the following orientations: $TiC(111)\|Al_2O_3(0001)$, $TiC\langle 110\rangle\|Al_2O_3\langle\bar{1}100\rangle$ and $Ti_2AlC(0001)\|Al_2O_3(0001)$, $Ti_2AlC\langle\bar{1}2\bar{1}0\rangle\|Al_2O_3\langle\bar{1}100\rangle$. A significant amount of oxygen was incorporated into the structure as measured by elastic recoil detection analysis, (see Ref. 12 for details).

A cross-sectional sample for scanning transmission electron microscopy (STEM) was prepared by conventional methods followed by low-angle Ar-ion milling. A VG601 STEM operated at 100 kV and a Gatan Enfina spectrometer was used for imaging and EELS spectrum imaging. For spectroscopy, an objective aperture allowing for 11 mrad convergence angle and a collector aperture allowing for 2 mrad acceptance angle were used. Spectrum images were recorded in low-loss and core-loss regions and the core-loss spectrum image was subsequently deconvolved for multiple scattering using the Fourier-ratio method. Determination of the relative oxygen concentration was performed using the GATAN DIGITAL MICROGRAPH software and the oxygen con-

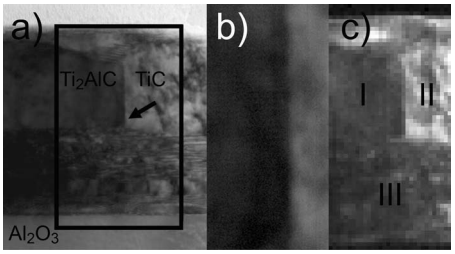

FIG. 1. (a) BF STEM image of a cross-sectional sample where the frame highlights the area used for EELS spectrum imaging. Also indicated is the grain boundary between Ti_2AlC *MAX* phase and TiC. The same boundary is magnified in (b), visualizing the *c* axis lattice fringes in the Ti_2AlC. The Ti $L_{2,3}$ spectrum image is shown in (c) with the Ti_2AlC, TiC and mixed regions indicated as I, II, and III.

tent was estimated to 5–10 at % depending on the choice of cross-section model, background, and signal widths.

The WIEN2K code[19] was used to calculate the electronic structure (site- and symmetry-projected density of states, PDOS) of the Ti_2AlC and TiC, where oxygen was substituting for aluminum or carbon in the *MAX* phase and for carbon in TiC. Oxygen substituting for titanium was not simulated because the titanium concentration remains near 50 at % in these films even though they contain 15 at % oxygen.[12]

An appropriate supercell was chosen based on the criterion to mimic a random alloy. This can be achieved by simulating a solid solution of C and O on the C sublattice by the so-called special quasirandom structure method.[20] By looking at the convergence in total energy for various oxygen configurations in $Ti_2AlC_{0.5}O_{0.5}$, a supercell based on $2\times2\times1$ unit cells with a total of 32 atoms were chosen for both the Ti_2AlC and TiC structures. The oxygen concentration was then varied by placing one, two, or four oxygen atoms in the supercell. When replacing carbon in Ti_2AlC, the positions were (0,0,0), (1/2,1/2,0), (0,1/2,1/2), and (1/2,0,1/2) while for aluminum they were (1/3,1/6,1/4), (5/6,2/3,1/4), (2/3,1/3,1/4), and (1/6,5/6,1/4). For TiC, the corresponding carbon positions were (1/4,1/4,1/2) (3/4,3/4,1/2), (1/4,3/4,1/2), and (3/4,1/4,1/2). This resulted in ~3.1, 6.2, and 12.5 at % O in the cells. The cells were then subject to relaxation of internal structural parameters such that the forces were less than 2 mRy/Bohr. Finally, the energy-loss near-edge structure (ELNES) spectra of these structures were simulated, given the known experimental conditions, and broadened by a Gaussian function to account for system broadening. For all calculations, the exchange-correlation potential of Perdew *et al.*[21] was used. The *l* expansion of the nonspherical potential and charge density inside the muffin-tin (MT) spheres was limited to $l_{max}=12$. The plane waves were cut off at a k_{max} such that $R_{MT}k_{max}=7$, where R_{MT} is the average radius for the MT spheres. The number of *k* points in the Brillouin zone was set to 2000, based on test calculations showing that more *k* points only give a minor change in the DOS, which is not visible in the energy-loss spectrum. A self-consistency cycle was iteratively converged until the energy difference between iterations was less than 0.1 meV.

Figure 1 shows the STEM and EELS imaging results. The bright field (BF) STEM image in Fig. 1(a) shows a cross

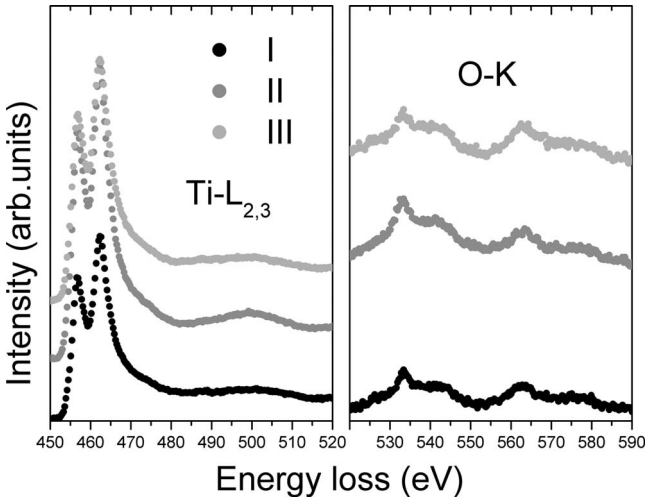

FIG. 2. The averaged background-subtracted and deconvolved spectrum image data from regions I-III, for the Ti $L_{2,3}$ and O *K* edges.

section of the film, with the Al_2O_3 substrate at the bottom of the image and the film on top. The film exhibits a varying structure near the substrate with an abundance of stacking faults. This region is composed of both cubic TiC and hexagonal Ti_2AlC stacked in a random order as determined by transmission electron microscopy. This mixed layer is followed by two crystalline grains (one dark and one bright) separated by a sharp boundary. The inserted frame in Fig. 1(a) indicates the region used for collection of the EELS spectrum image. A higher magnification image of the boundary between the two grains is presented in Fig. 1(b). From this image it can be seen that the dark grain contains lattice fringes with about 1 nm spacing whereas the bright grain does not. Based on the known epitaxial relationships, the fringe structure identifies the Ti_2AlC while the bright grain is TiC. Finally, Fig. 1(c) shows the background-subtracted and multiple-scattering-deconvolved titanium $L_{2,3}$ core-loss spectrum image. Here it can be seen that the grains indicated in Fig. 1(a) provide enough contrast to be identified also in the spectrum image. Consequently, all individual spectra in these different regions were averaged to reduce the spectrum noise and treated as three different spectra, from Ti_2AlC, TiC, and a mixture thereof, in regions I, II, and III, respectively.

The ELNES information as acquired from the spectrum image is shown in Fig. 2, revealing the appearance of the Ti $L_{2,3}$ and O *K* edges in regions I-III. The difference in the fine structure and relative intensity of the O *K* edge between these regions is negligible. A stronger intensity can be seen for II, which is related to the more weakly diffracting (hence brighter BF image) TiC grain. Normalizing the spectra (I-III) gives identical intensities of both Ti and O edges (not shown). The appearance of the fine structure is not purely O *K* as it appears to be superimposed on Ti $L_{2,3}$ far-edge peaks. Furthermore, the Ti L_1 peak is located at 563 eV. The spectra suggest two things: that the chemical environment of the oxygen atoms is similar for both Ti_2AlC and TiC and that the oxygen is uniformly distributed in the film without preference for segregation to either phase looking at the O *K* edge with onset at 531 eV. Disregarding the superimposed

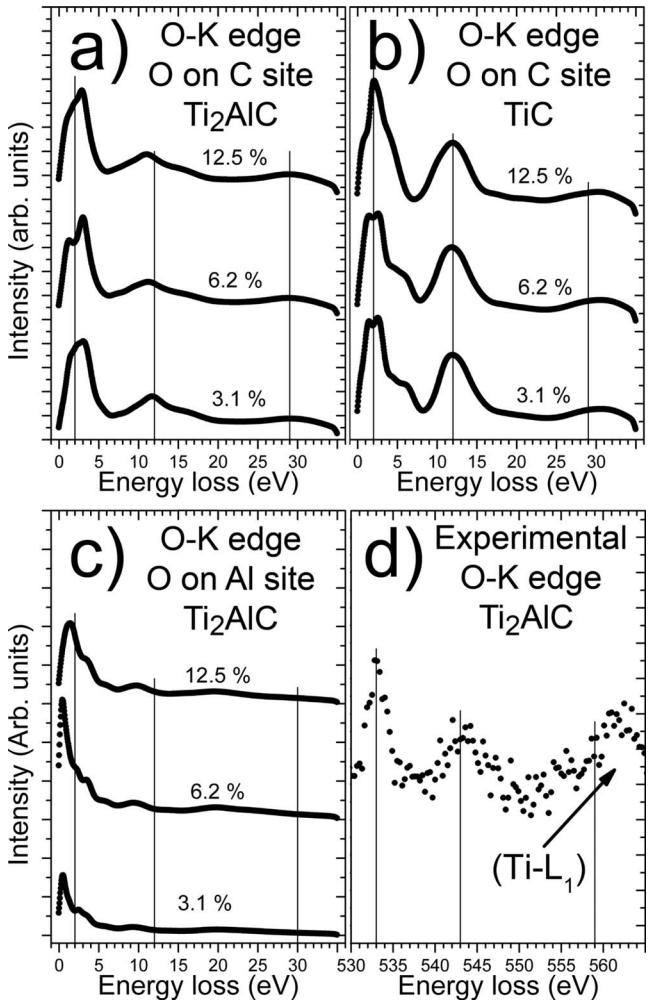

FIG. 3. [(a)–(c)] Calculated O *K* edge spectra for the various structures, substitutional sites, and oxygen concentrations. (d) For comparison: the experimentally acquired Ti $L_{2,3}$ subtracted O *K* spectrum. The vertical lines in [(a)–(d)] indicate the positions of 2, 12, and 30 eV after the edge onset, to highlight the shift and positions of respective peaks.

features from the Ti $L_{2,3}$ edges, and the additional Ti L_1 peak, the O *K* edge is characterized by a sharp peak centered at 533 eV followed by a less pronounced peak centered about 10 eV after the first peak.

The simulated ELNES spectra are shown in Figs. 3(a)–3(c) for the different oxygen concentrations, materials, and substitutional sites. For comparison, the experimentally obtained O *K* edge from Ti_2AlC, with subtracted Ti $L_{2,3}$ far-edge peak, is shown in Fig. 3(d). For (a) and (b) where oxygen is replacing carbon, the spectra appear rather similar. An initial distinctive peak, centered at ~2 eV from the edge onset, is followed by two broader and more shallow peaks at ~12 and ~30 eV after the edge onset. The fine structure, however, reveals differences between the two. The second peak is stronger in TiC than in Ti_2AlC and there is a small shift of the second peak for the *MAX* phase with increasing oxygen concentration. Looking at (c) however, where oxygen is replacing aluminum in Ti_2AlC, the spectrum differs in appearance from the previous two. It is characterized by an initial sharp and narrow peak with near exponentially decreasing intensity, and weak peaks, e.g., at 10 eV after the onset. This is in contrast to the experimental O *K* edge, where two peaks can be identified at ~2 and ~12 eV after the edge onset, neglecting the Ti L_1 peak at ~32 eV after the edge.

The experimentally obtained Ti_2AlC peak positions are identical to those in the calculated spectra for oxygen on carbon sites. The peak widths also match while peak heights correspond better to the TiC calculation. The peak heights are, however, strongly dependent on the correct removal of the Ti $L_{2,3}$ peak. It is not surprising that the calculated spectra, for $Ti_2Al(O,C)$ and Ti(O,C), appear so similar, since the oxygen in both these cases is surrounded by an octahedron of titanium atoms. In contrast, the coordination of the titanium atoms around the aluminum site is trigonal prismatic.

The close resemblance of experimentally acquired O *K* spectra from Ti_2AlC and TiC, as well as the simulated spectra of oxygen on carbon sites for these materials, leads us to conclude that oxygen substitutes for carbon in both the Ti_2AlC and the TiC structures. It further leads us to conclude that the Ti_2AlC material investigated is actually a *MAX*-phase oxycarbide; *MA*(O,C) and that O is a third *X* element. Having a third *X* element increases the parameter space of the possible *MAX* combinations significantly.

The above results are not surprising given the preference for oxygen to reside on a carbon site in TiC. TiC and TiO both have the same fcc structure (space group 225_*Fm*3*m*) and nearly identical lattice parameters (4.330 and 4.293 Å, respectively). This allows for easy alloying of an oxycarbide Ti(O,C) with a presumably complete miscibility. Considering the same octahedral environment of the carbon atom in Ti_2AlC, it is surprising that *MAX*-phase oxycarbides have not been reported in the past. Now that these alloys have been identified, the full-alloying miscibility between *MA*(C) and *MA*(O) phases expands the *MAX* permutation space, and the associated materials properties are available for exploration.

In conclusion, we have provided evidence that oxygen is as easily incorporated on the carbon site in the Ti_2AlC *MAX* phase as in TiC. This leads to the conclusion that oxygen is a third *X* element in addition to C and N. The here presented finding also identifies the possibility of growth of *MA*(C,O) oxycarbides with notable changes in materials properties. Given the complete miscibility of TiC and TiO, the possibility of a *MA*(O) phase cannot be excluded.

P.O.Å. Persson wishes to acknowledge the Royal Swedish Academy of Sciences for financial support. J. Rosén acknowledges financial support from the Swedish Foundation for Strategic Research. The Australian Research Council (ARC) is gratefully acknowledged for project funding.

[1] V. H. Nowotny, Prog. Solid State Chem. **5**, 27 (1971).
[2] M. W. Barsoum, Prog. Solid State Chem. **28**, 201 (2000).
[3] H. B. Zhang, Y. W. Bao, and Y. C. Zhou, J. Mater. Sci. Technol. **25**, 1 (2009).
[4] M. W. Barsoum and T. El-Raghy, Am. Sci. **89**, 334 (2001).
[5] J.-P. Palmquist, O. Wilhelmsson, U. Jansson, J. Emmerlich, P. O. Å. Persson, H. Högberg, L. Hultman, S. Li, R. Ahuja, and O. Eriksson, Phys. Rev. B **70**, 165401 (2004).
[6] J. Rosén, L. Ryves, P. O. Å. Persson, and M. M. M. Bilek, J. Appl. Phys. **101**, 056101 (2007).
[7] H. Nowotny, P. Rogl, and J. C. Schuster, J. Solid State Chem. **44**, 126 (1982).
[8] B. Manoun, S. K. Saxena, G. Hug, A. Ganguly, E. N. Hoffman, and M. W. Barsoum, J. Appl. Phys. **101**, 113523 (2007).
[9] Z. M. Sun, R. Ahuja, and J. M. Schneider, Phys. Rev. B **68**, 224112 (2003).
[10] F. L. Meng, Y. C. Zhou, and J. Y. Wang, Scr. Mater. **53**, 1369 (2005).
[11] M. W. Barsoum, M. Ali, and T. El-Raghy, Metall. Mater. Trans. A **31**, 1857 (2000).
[12] P. O. Å. Persson, J. Rosén, D. R. McKenzie, M. M. M. Bilek, and C. Höglund, J. Appl. Phys. **103**, 066102 (2008).
[13] J. Rosén, P. O. Å. Persson, M. Ionescu, A. Kondyurin, D. R. McKenzie, and M. M. M. Bilek, Appl. Phys. Lett. **92**, 064102 (2008).
[14] S. Shimada and M. Kozeki, J. Mater. Sci. **27**, 1869 (1992).
[15] L. S. A. Marques, A. C. Fernandes, F. Vaz, and M. D. Ramos, Plasma Processes Polym. **4**, S195 (2007).
[16] N. I. Medvedeva, D. L. Novikov, A. L. Ivanovsky, M. V. Kuznetsov, and A. J. Freeman, Phys. Rev. B **58**, 16042 (1998).
[17] T. Liao, J. Wang, and Y. Zhou, Appl. Phys. Lett. **93**, 261911 (2008).
[18] L. Ryves, M. M. M. Bilek, T. W. H. Oates, R. N. Tarrant, D. R. McKenzie, F. A. Burgmann, and D. G. McCulloch, Thin Solid Films **482**, 133 (2005).
[19] P. Blaha, K. Schwarz, G. K. H. Madsen, D. Kvasnicka, and J. Luitz, *Wien2k, An Augmented Plane Wave+Local Orbitals Program for Calculating Crystal Properties*, edited by K. Schwarz (Universität Wien, Austria, 2001).
[20] A. Zunger, S. H. Wei, L. G. Ferreira, and J. E. Bernard, Phys. Rev. Lett. **65**, 353 (1990).
[21] J. P. Perdew, K. Burke, and M. Ernzerhof, Phys. Rev. Lett. **77**, 3865 (1996).